



# Loss of Microglial Parkin Inhibits Necroptosis and Contributes to Neuroinflammation

Pedro Elói Antunes Dionísio<sup>1</sup> · Sara Rodrigues Oliveira<sup>1</sup> · Joana São José Dias Amaral<sup>1</sup> · Cecília Maria Pereira Rodrigues<sup>1</sup> 

Received: 14 May 2018 / Accepted: 18 July 2018 / Published online: 3 August 2018  
© Springer Science+Business Media, LLC, part of Springer Nature 2018

## Abstract

Parkin is an E3 ubiquitin ligase involved in Parkinson's disease (PD). Necroptosis is a regulated form of cell death that depends on receptor interacting protein 1 (RIP1) and 3 (RIP3). Importantly, parkin has been implicated in ubiquitination events that can alter inflammation and necroptosis. Here, we investigated how parkin influences microglial function. Incubation of BV-2 microglial cells with zVAD.fmk (zVAD) induced high levels of cell death and viability loss, while N9 microglial cells and primary microglia required further stimuli. Importantly, necrostatin-1 (Nec-1), an inhibitor of RIP1 kinase activity, abrogated cell death, thus implicating RIP1-dependent necroptosis in cell death. Cell death was characterized by necrosome assembly, as determined by sequestration of RIP1/RIP3 in insoluble fractions and by MLKL phosphorylation, which were all abolished by Nec-1. Also, necroptosis-inducing conditions led to TNF- $\alpha$  secretion, which may in turn contribute to autocrine necroptosis activation. Interestingly, parkin knockdown protected BV-2 cells from zVAD-induced necroptosis, which may depend on the higher RIP1 ubiquitination levels detected in siRNA-PARK2 transfected cells. This effect was independent of inflammation, since pro-inflammatory stimulation of BV-2 and primary microglia with silenced parkin resulted in stronger pro-inflammatory gene expression, an opposite observation from zVAD-exposed BV-2 cells. LPS-mediated inflammation was exacerbated by NF- $\kappa$ B/JNK over-activation. Finally, no alterations in mitochondrial ROS production were detected in any condition, thereby excluding the role of parkin in mitophagy. In conclusion, here, we reveal that parkin may have unsuspected roles in microglia by modulating ubiquitination. Parkin loss exacerbates inflammation and promotes survival of activated microglia, thus contributing to chronic neuroinflammation.

**Keywords** Inflammation · Microglia · Necroptosis · Parkin · Ubiquitination

## Introduction

Parkinson's disease (PD) is mainly caused by dopaminergic neurodegeneration in the *substantia nigra pars compacta* [1]. PD etiology is complex, involving oxidative stress, mitochondrial dysfunction, and chronic neuroinflammation [1]. Although mostly sporadic, 5–10% of all cases are related to

heritable forms of PD [1, 2]. In this regard, loss-of-function mutations in the *PARK2* gene, which encodes for the ubiquitous cytosolic ring between ring E3 ubiquitin ligase parkin, is associated with juvenile autosomal-recessive PD [1, 2]. Heterozygous carriers of these mutations present a higher risk of developing the disease [3]. Moreover, parkin can be inactivated by several pathological features involved in sporadic PD, such as oxidative stress [4].

Parkin is involved in the mitophagy of depolarized/damaged mitochondria [1, 5]. However, new roles have been ascribed for parkin, which can mediate degradative and non-degradative ubiquitination signaling [5, 6]. For example, parkin can increase linear ubiquitin chain assembly complex (LUBAC) activity, leading to NF- $\kappa$ B activation [6, 7]. Moreover, parkin contributes to different ubiquitination processes, which include linkages between lysine-63 (Lys63) involved in signaling, or between lysine-48 (Lys48), which target proteins for proteasomal degradation [4]. Further, parkin may be involved in the regulation of the inflammatory response. *PARK2*

---

**Electronic supplementary material** The online version of this article (<https://doi.org/10.1007/s12035-018-1264-9>) contains supplementary material, which is available to authorized users.

---

✉ Joana São José Dias Amaral  
jamaral@ff.ulisboa.pt

✉ Cecília Maria Pereira Rodrigues  
cmprodrigues@ff.ulisboa.pt

<sup>1</sup> Research Institute for Medicines (iMed.U LISBOA), Faculty of Pharmacy, Universidade de Lisboa, 1649-003 Lisbon, Portugal

polymorphisms are associated with leprosy susceptibility [8], while its downregulation appears to decrease pro-inflammatory induction in stimulated macrophages [9, 10]. Conversely, macrophages derived from parkin-null mice express higher levels of pro-inflammatory agents [11]. Moreover, parkin targets tumor necrosis factor  $\alpha$  (TNF- $\alpha$ ) receptor (TNFR)-associated factor 2 (TRAF2) and 6 (TRAF6) to proteasomal degradation [12]. Although controversial, these findings suggest an interplay between parkin and inflammation.

Polyubiquitination also regulates the cross-talk between inflammation, survival, and death [6, 13, 14]. Necroptosis is a caspase-independent form of regulated cell death typically executed via activation of receptor-interacting protein 3 (RIP3) and RIP1, being negatively regulated by caspase-8 [14, 15]. RIP1 activation usually depends on transmembrane receptor stimulation, such as TNFR1, Toll-like receptor 3 (TLR3) and TLR4 [14–16]. Upon receptor stimulation, RIP1 is recruited to complex I, where it is polyubiquitinated by the E3-ubiquitin ligases cellular inhibitor of apoptosis (cIAPs) and LUBAC. These ubiquitin chains stabilize complex I and signal towards NF- $\kappa$ B and mitogen-associated protein kinase (MAPKs) activation [14, 15, 17]. However, upon deubiquitination, complex I dissociates, which may lead to insoluble amyloid-like necrosome assembly between RIP1 and RIP3, and RIP3-dependent phosphorylation of the mixed lineage kinase domain-like protein (MLKL) at T357/S358 [14, 15, 18, 19]. Then, MLKL oligomerizes and translocates to cellular membranes, leading to membrane disruption [14, 15, 19]. Importantly, necroptosis has been implicated in neurodegenerative diseases, including Alzheimer's disease [20] and, more recently, PD [21].

We hypothesized that parkin plays unsuspected roles in PD pathogenesis by modulating inflammation and necroptosis in microglia. Surprisingly, parkin knockdown protected from zVAD.fmk (zVAD)-mediated necroptosis, probably by indirectly increasing RIP1 polyubiquitination. Moreover, loss of parkin exacerbated LPS-driven inflammatory response by over-activating c-Jun N-terminal kinase (JNK) and NF- $\kappa$ B pathways. Of note, mitochondrial reactive oxygen species (ROS) were not altered after parkin modulation. Furthermore, we characterized how multiple stimuli can induce necroptosis in mouse BV-2, N9, and primary microglia, which will contribute to further dissect the complex aspects linking inflammation and cell death in microglia.

## Materials and Methods

### Cell Culture and Reagents

BV-2 and N9 mouse microglial cell lines were kindly provided by Dr. Elsa Rodrigues (University of Lisbon). The BV-2 cell line was immortalized from primary microglia cultures derived from C57BL/6 mouse pups infected with a J2

retrovirus [22], while the N9 cell line was established from brain primary cultures derived from CD1 mouse embryos infected with a 3RV retrovirus [23]. We used the commonly studied BV-2 and N9 mouse microglial cell lines, which are derived from the inbred C57BL/6 and outbred CD1 mouse strains, respectively, in order to characterize their necroptotic responses and compare them to primary C57BL/6 primary microglia. Of note, these cell lines react with different intensities to the same inflammatory stimuli, which has been linked to differences in the immune responses detected in the original mouse strains [24]. Both cell lines were maintained in RPMI 1640 medium (GIBCO Life Technologies, Inc. Grand Island, USA), supplemented with 10% heat inactivated fetal bovine serum (FBS), 1% antibiotic/antimycotic solution and 1% GlutaMAX™ (all from GIBCO).

Primary microglia were obtained from mixed glial cultures [25], with minor modifications. Briefly, mixed glial cultures were prepared from meninge-free cortices of 2–3-day-old C57BL/6 mouse pups. Individualized cells were obtained by mechanical fragmentation followed by sequential passages through steel screens of 230-, 104-, and 74- $\mu$ m pore sizes. Cells were plated at  $4 \times 10^5$  cells/cm<sup>2</sup> on 75-cm<sup>2</sup> or 25-cm<sup>2</sup> culture flasks in DMEM-F12 + GlutaMAX™ medium supplemented with 10% FBS and 1% antibiotic/antimycotic (GIBCO). Both microglial cell lines and primary cultures were maintained at 37 °C in a humidified atmosphere of 5% CO<sub>2</sub>.

Isolation of microglia was performed as described before [26]. In brief, after 21–25 days in vitro, the upper layer containing astrocytes was detached by mild trypsinization with a 0.25% trypsin-1 mM EDTA solution (GIBCO) diluted 1:3 in DMEM-F12 for 30–45 min and then discarded, whereas microglia remained attached to the flasks. Afterwards, microglia were trypsinized with trypsin-EDTA for 10 min and collected following vigorous pipetting. Microglia that remained attached were further collected with a cell scraper. Finally, microglial cells were plated at  $5 \times 10^4$  cells/cm<sup>2</sup> in mixed glial culture-conditioned medium previously centrifuged at 600g for 5 min and allowed to rest for 2 days before being manipulated. Astrocyte contamination was less than 1%, as determined by immunocytochemistry with a primary antibody for glial fibrillary acidic protein (GFAP) (GA5; Millipore), a marker of astrocytes, and Iba-1 (Wako Pure Chemicals), a marker of microglia (Supplementary Fig. 1).

For both microglial cell lines and primary cultures, treatments were performed in serum-free medium (RPMI 1640 or DMEM-F12, respectively), supplemented with 1% antibiotic/antimycotic solution, 1% insulin-transferrin-selenium (ITS-G supplement, GIBCO), and 1 mg/mL bovine serum albumin (BSA) fraction V (7.5% solution, GIBCO) [27]. The reagents used were as follows: lipopolysaccharide (LPS) from *Escherichia coli* 055:B5 (#437625, Calbiochem); necrostatin-1 (Nec-1) (#N9037, Sigma-Aldrich, St. Louis, MO, USA); zVAD pan caspase inhibitor (#ALX-260-020, Enzo Life

Sciences, Farmingdale, NY, USA) zIETD.fmk (IETD) caspase-8 inhibitor (#FMK007, R&D Systems, Minneapolis, USA); BV6 Smac mimetic (#B4653, ApexBio, Houston, USA); recombinant murine TNF- $\alpha$  (#315-01A, PeproTech EC Ltd., London, UK); recombinant murine interferon- $\gamma$  (IFN $\gamma$ ) (#315-05, Peprotech), and N-acetyl-L-cysteine (Nac) (#A7250, Sigma-Aldrich).

### siRNA Transfection

All transfections were performed with Lipofectamine 3000 (Invitrogen, Life Technologies), according to the manufacturer's instructions. For siRNA-mediated downregulation of parkin, the siGENOME SMARTpool Mouse Park2 siRNA (#M-065413-01-0005, Dharmacon) was used at 50 nM, while the siGENOME Non-Targeting siRNA Pool #1 (#D-001206-13-05) was used as control. Transfection of siRNAs was maintained for 48 h before further treatments.

### Cell Death/Survival Determination

For evaluation of cell death and viability, BV-2 and N9 cells were plated in 96-well plates at  $7 \times 10^3$  cells/well for next-day treatments of 8 and 24 h, or at  $3 \times 10^3$  cells/well for transfection. General cell death was evaluated using the lactate dehydrogenase (LDH) Cytotoxicity Detection Kit<sup>PLUS</sup> (Roche Diagnostics GmbH, Mannheim, Germany), by determining the quantities of cytosolic LDH derived from cells with permeabilized plasma membranes present in the extracellular medium. In brief, 50  $\mu$ L of culture supernatant from each well was added to a new 96-well plate to evaluate LDH release. Concomitantly, cells on the original plate were lysed for 10 min with agitation in lysis solution diluted 1:20 in 50  $\mu$ L of medium, to determine the amount of intracellular LDH. Afterwards, supernatant samples and cell lysates were incubated with 50  $\mu$ L of assay substrate for approximately 30 min, at room temperature, protected from light. Absorbance readings were measured at 490 nm, with 620 nm reference wavelength in a Model 680 microplate reader (Bio-Rad, Hercules, CA, USA). The percentage of LDH release was calculated as the ratio between the released LDH (contained in the supernatant) and the total LDH (supernatant + cell lysate), as previously described [28].

MTS metabolism was evaluated as an indicator of cell viability using the CellTiter 96 AQueous non-radioactive cell proliferation assay (Promega, Madison, WI, USA), according to the manufacturer's instructions. Changes in absorbance were measured at 490 nm, using a Model 680 microplate reader (Bio-Rad).

### Total and Soluble/Insoluble Protein Extraction

For total protein extraction, BV-2 and N9 cells were plated in 35-mm dishes at  $2.5 \times 10^5$  cells/dish for next-day treatment or at  $1.1 \times 10^5$  cells/dish for transfection. Floating cells were

collected by centrifugation at 600g for 5 min and the pellet was dissolved in lysis buffer containing 10 mM Tris-HCl (pH 7.6), 2.5 mM MgCl<sub>2</sub>, 0.75 mM KAc, 0.5% nonyl phenoxyethoxyethanol (NP-40), 1 mM dithiothreitol (DTT), and 1 $\times$  Halt protease and phosphatase inhibitor cocktail (EDTA-free, Pierce, Thermo Fisher Scientific, Rockford, IL, USA), which was further used to scrape adherent cells directly. The samples were allowed to rest on ice for 30 min. After, cell lysates were then sonicated and centrifuged at 3200g for 10 min at 4  $^{\circ}$ C and the supernatants were recovered. Total protein extracts were stored at  $-80$   $^{\circ}$ C. Protein concentrations were calculated from the colorimetric Bradford method by using the Bio-Rad protein assay kit, according to the manufacturer's recommendations. Soluble and insoluble fractions were isolated as described in [29]. Briefly, floating and adherent cells were collected directly in NP-40 lysis buffer (1% NP-40, 20 mM Tris-HCl pH 7.4, 150 mM NaCl, 5 mM EDTA, 10% glycerol, 1 mM DTT, and 1 $\times$  Halt protease and phosphatase inhibitor cocktail). Lysates were then rotated for 30 min at 4  $^{\circ}$ C and then centrifuged at 16,000g for 20 min at 4  $^{\circ}$ C. Supernatants were recovered and used as the soluble fractions. To remove carry-overs, the pellet was washed with NP-40 lysis buffer and further centrifuged at 16,000g for 10 min at 4  $^{\circ}$ C. Then, the pellet was resuspended in urea-sodium dodecyl sulfate (SDS) buffer (8 M urea, 3% SDS in NP-40 lysis buffer) followed by sonication. Lysates were centrifuged at 16,000g for 20 min at 4  $^{\circ}$ C, and the supernatants were used as the detergent-insoluble fractions. Protein concentration was determined using the bicinchoninic acid (BCA) assay (Thermo Fisher Scientific, Inc.), according to the manufacturer's instructions.

### Western Blot Analysis

Equal amounts of protein (50  $\mu$ g) were denatured and resolved on 8% SDS-PAGE gels. The resolved proteins were transferred onto nitrocellulose membranes and blocking was performed with a 5% nonfat dried milk solution. Membranes were then incubated overnight at 4  $^{\circ}$ C with agitation with the following primary rabbit antibodies: RIP3; NF- $\kappa$ B; I $\kappa$ B (#135170, #372, #371, Santa Cruz Biotechnology); MLKL (#M6697, Sigma-Aldrich); p-MLKL (Ser358) (#196436, Abcam; Cambridge, UK); RIP1; p-p38 (Thr180/Tyr182); Erk1/2 (#3493, #9211, #4695, Cell Signaling; MA, USA); and with the following mouse monoclonal antibodies: JNK; p-JNK (Thr183/Tyr185); p38 $\alpha$ / $\beta$ , p-Erk1/2 (Tyr204); ubiquitin (#7345, #6254, #7972, #7383, #8017, Santa Cruz Biotechnology); and p-I $\kappa$ B (Ser32/36) (#9246, Cell Signaling). The membranes were then incubated with goat secondary antibodies conjugated with horseradish peroxidase anti-mouse or anti-rabbit (Bio-Rad Laboratories, Hercules, CA, USA) for 2 h at room temperature. After rinsing 3 $\times$  with TBS/0.2% Tween 20, the immunoreactive proteins were visualized with Immobilon<sup>TM</sup> Western (Millipore) or SuperSignal West Femto substrate (Thermo

Scientific).  $\beta$ -actin (AC-15, Sigma-Aldrich) was used as loading control. Densitometric analyses were performed with the Image Lab software Version 5.1 Beta (Bio-Rad).

### Immunoprecipitation

RIP1 ubiquitination levels were determined by immunoprecipitation of RIP1 followed by immunoblot detection of ubiquitin. In brief, BV-2 cells were plated in 6-cm dishes at  $1 \times 10^6$  cells/dish and transfected on the following day for 48 h before exposure to zVAD for 5 h. Then, cells were lysed in RIPA buffer (50 mM Tris-HCl, pH 8, 150 mM NaCl, 1% NP-40, 0.5% deoxycholic acid, 0.1% SDS) with sonication, and 300  $\mu$ g of protein in 200  $\mu$ l RIPA buffer were pre-cleared with G-linked agarose beads (Ezview Red Protein G Affinity Gel, #E3403, Sigma-Aldrich) for 3 h at 4 °C with rotation. After, samples were rotated overnight at 4 °C with either RIP1 antibody (#3493, Cell Signaling) 1:200 or with the same concentration of non-specific rabbit IgGs as negative control. Next, samples were incubated with G agarose beads overnight at 4 °C with rotation. On the next day, beads were pulled down, washed 3 $\times$  with RIPA buffer, and resuspended in denaturing buffer and heated at 95 °C for 5 min to elute the bound proteins. Beads were pulled down and the samples were processed for western blot analysis as described previously.

### Sandwich ELISA

Sandwich ELISA kits (#900-K54 plus PeproTech's ELISA Buffer kit #900-600, PeproTech) were used to determine TNF- $\alpha$  concentration in 100  $\mu$ L of previously centrifuged (600g for 5 min at 4 °C) cell culture supernatant, according to the manufacturer's indications.

### Real-Time PCR

For RNA extraction, BV-2 cells were plated in 12-well plates at  $4 \times 10^4$  cells/well and transfected on the following day for 48 h before exposure to LPS or zVAD for 8 h. Primary microglia were plated in 6-well plates at  $5 \times 10^5$  cells/well and transfected after 2 days for 48 h before exposure to either 100 ng/mL LPS, 10 ng/mL TNF- $\alpha$ , 100 U/mL IFN $\gamma$ , or TNF- $\alpha$  + IFN $\gamma$  for 8 h. Then, adherent cells were washed once with PBS and TRIzol™ reagent (Invitrogen, Grand Island, USA) was added directly. For zVAD conditions, the correspondent floating cells were collected by centrifugation and resuspended in the same TRIzol sample. After, total RNA was isolated according to the manufacturer's protocol and quantified using a Qubit™ 2.0 fluorometer (Invitrogen). Total RNA was converted into cDNA using NZY Reverse Transcriptase (NZYTech, Lisbon, Portugal), according to the manufacturer's instructions. Quantitative real-time PCR (qRT-PCR) analyses were performed in the 7300 real-time PCR

System (Applied Biosystems, Foster City, CA, USA), in a final volume of 12.5  $\mu$ L using 2 $\times$  SYBR Green PCR master mix and 0.3  $\mu$ M of each primer pair (Fermentas International Inc., Glen Burnie, Maryland, USA). The expression levels of the genes of interest relative to the housekeeping gene hypoxanthine-guanine phosphoribosyltransferase (HPRT) were calculated using the relative standard curve method. Primer sequences are presented in Supplementary Table 1.

### NF- $\kappa$ B Transcriptional Activity Assay

NF- $\kappa$ B transcriptional activity was determined using the Cignal NF- $\kappa$ B Pathway Reporter Assay Kit (#CCS013L, QIAGEN, Chatsworth, CA, USA), according to the manufacturer's instructions. Briefly, BV-2 cells were plated in 96-well plates at  $3 \times 10^3$  cells/well and transfected with either siRNA-Control or siRNA-PARK2. Following 24 h, medium was changed and cells were transfected for further 24 h with a NF- $\kappa$ B responsive construct, which encodes the firefly luciferase reporter gene and that constitutively expresses *Renilla* luciferase gene or a negative or positive control construct. After treatment with either LPS or zVAD for 8 h, cells were lysed and processed for the Dual-Luciferase™ Reporter Assay System.

### Statistical Analysis

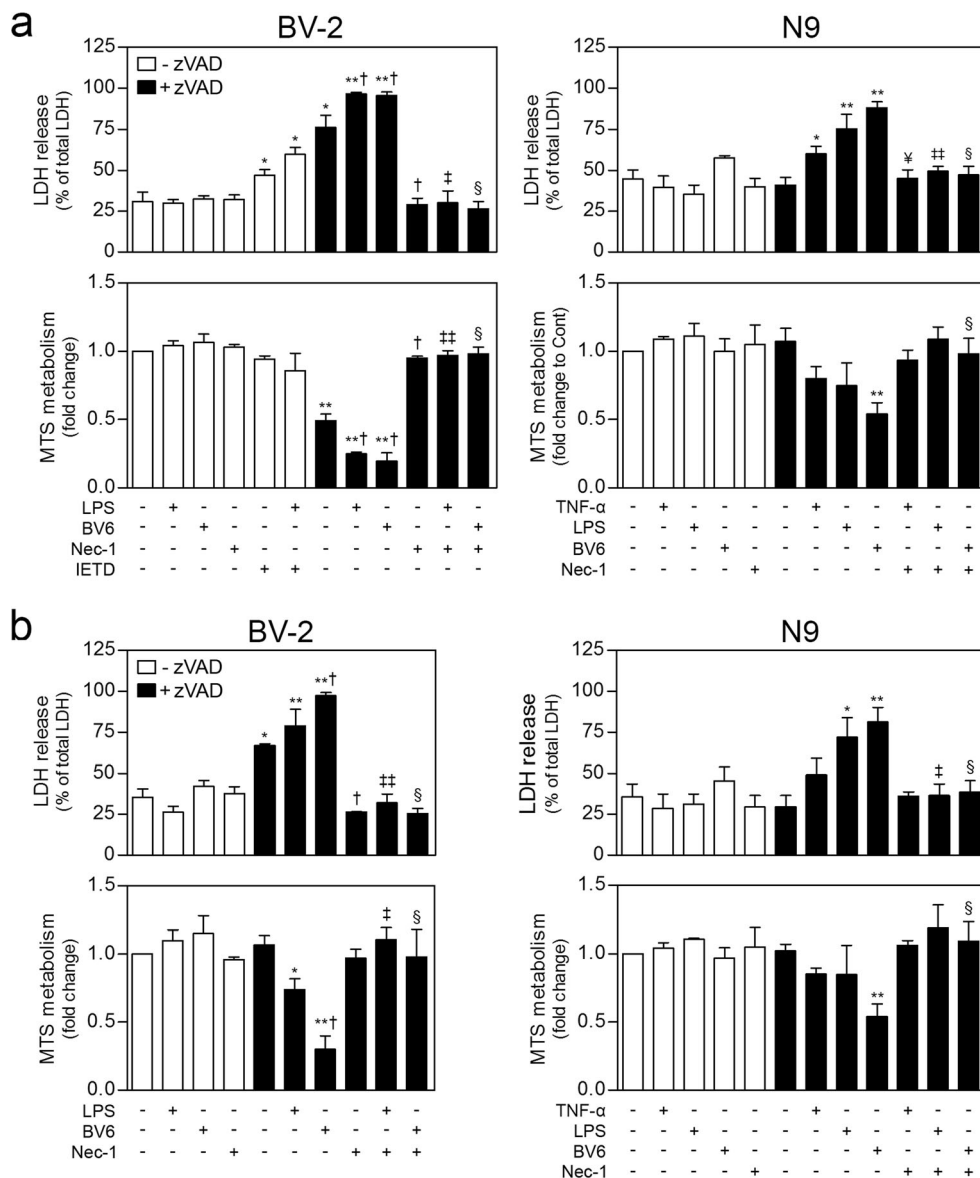
Data comparisons were conducted with one-way analysis of variance (ANOVA) followed by Tukey's or Bonferroni's post hoc tests as indicated.  $P < 0.05$  was considered statistically significant for all tests. Analyses and graphical presentation were performed with the GraphPad Prism Software Version 5 (GraphPad Software, Inc., San Diego, CA, USA). Results are presented as mean  $\pm$  standard error of the mean (SEM).

## Results

### Microglial Cells Undergo RIP1-Dependent Necroptosis after Caspase Inhibition

TLR3/4-stimulated primary murine microglia undergo necroptosis upon caspase blockade [16, 30]. Here, BV-2 and N9 cells were treated with the pan-caspase inhibitor zVAD or the caspase-8 inhibitor IETD for 24 h along with combinations of TNF- $\alpha$ , LPS (TLR4 agonist), BV6 (Smac mimetic), or Nec-1 (necroptosis inhibitor). Interestingly, exposure to zVAD only was sufficient to induce high levels of cell death in BV-2 cells (Fig. 1a). Moreover, co-incubation of zVAD with LPS or BV6 strongly exacerbated the release of LDH to almost 100%, while leading to total loss of cell morphology (Supplementary Fig. 2a). Curiously, these effects appear to be zVAD specific, since incubation with 50  $\mu$ M IETD alone or with LPS only slightly increased LDH release. Importantly, Nec-1 co-

**Fig. 1** BV-2 and N9 microglial cells undergo RIP1-dependent necroptosis. BV-2 and N9 cells were exposed to combinations of the following stimuli: 25  $\mu$ M zVAD, 50  $\mu$ M IETD, 0.5  $\mu$ M BV6, 10 ng/mL TNF- $\alpha$ , 100 ng/mL LPS, and 30  $\mu$ M Nec-1 for either 24 h (a) or 8 h (b). Then, cell membrane permeability and cell metabolism were evaluated by LDH and MTS assays, respectively. Values represent mean  $\pm$  SEM of five independent experiments. \* $p$  < 0.05 and \*\* $p$  < 0.01 from control, † $p$  < 0.05 from zVAD, ‡ $p$  < 0.05, and §§ $p$  < 0.01 from LPS + zVAD, § $p$  < 0.01 from zVAD + BV6 and ¶ $p$  < 0.05 from TNF- $\alpha$  + zVAD in one-way ANOVA followed by Tukey's post hoc test



treatment fully reverted cell death in all conditions, thus implicating RIP1 kinase activity in cell death. In N9 cells, zVAD-dependent cell death only occurred when BV6 or LPS was added (Fig. 1a). Co-incubation of zVAD with TNF- $\alpha$  also induced cell death, but to a minimal extent, indicating that caspase inhibition is not sufficient to induce necroptosis. Finally, cell death was abrogated by Nec-1 in all conditions tested.

To characterize the chronological events leading to cell death, BV-2 and N9 cells were exposed to similar stimuli for only 8 h (Fig. 1b). zVAD alone was sufficient to increase LDH release by 40% in BV-2 cells, while having no effect on MTS metabolism. These results confirmed that pore formation at the cellular membrane and subsequent leakage of cytosolic contents constitutes an initial step in the necroptotic cascade [19, 31], while ROS production and mitochondrial dysfunction [32] appear to contribute to late-stage necroptosis [16, 19,

31]. When BV-2 cells were treated simultaneously with zVAD and LPS, the percentage of LDH release raised up to almost 80%, while MTS metabolism was already decreased, thus suggesting a stronger necroptotic setting in this condition. Co-incubation of zVAD with BV6 was the strongest stimulus, inducing LDH release and reduction of MTS metabolism at levels similar to 24-h exposure. Moreover, the 8-h time-point recapitulated the results for 24 h in N9 cells.

Since zVAD is able to induce autocrine production of TNF- $\alpha$  [33, 34], we evaluated TNF- $\alpha$  secretion by BV-2 and N9 cells following exposure to combinations of zVAD, LPS, BV6, and Nec-1 for 5 h (Fig. 2a). Both BV-2 and N9 cells secreted considerable basal amounts of TNF- $\alpha$  (268 and 170 pg/mL, respectively), considering that 10 pg/mL are sufficient to induce necroptosis in zVAD-sensitized L929 cells [33]. As expected, we observed an increment of TNF- $\alpha$

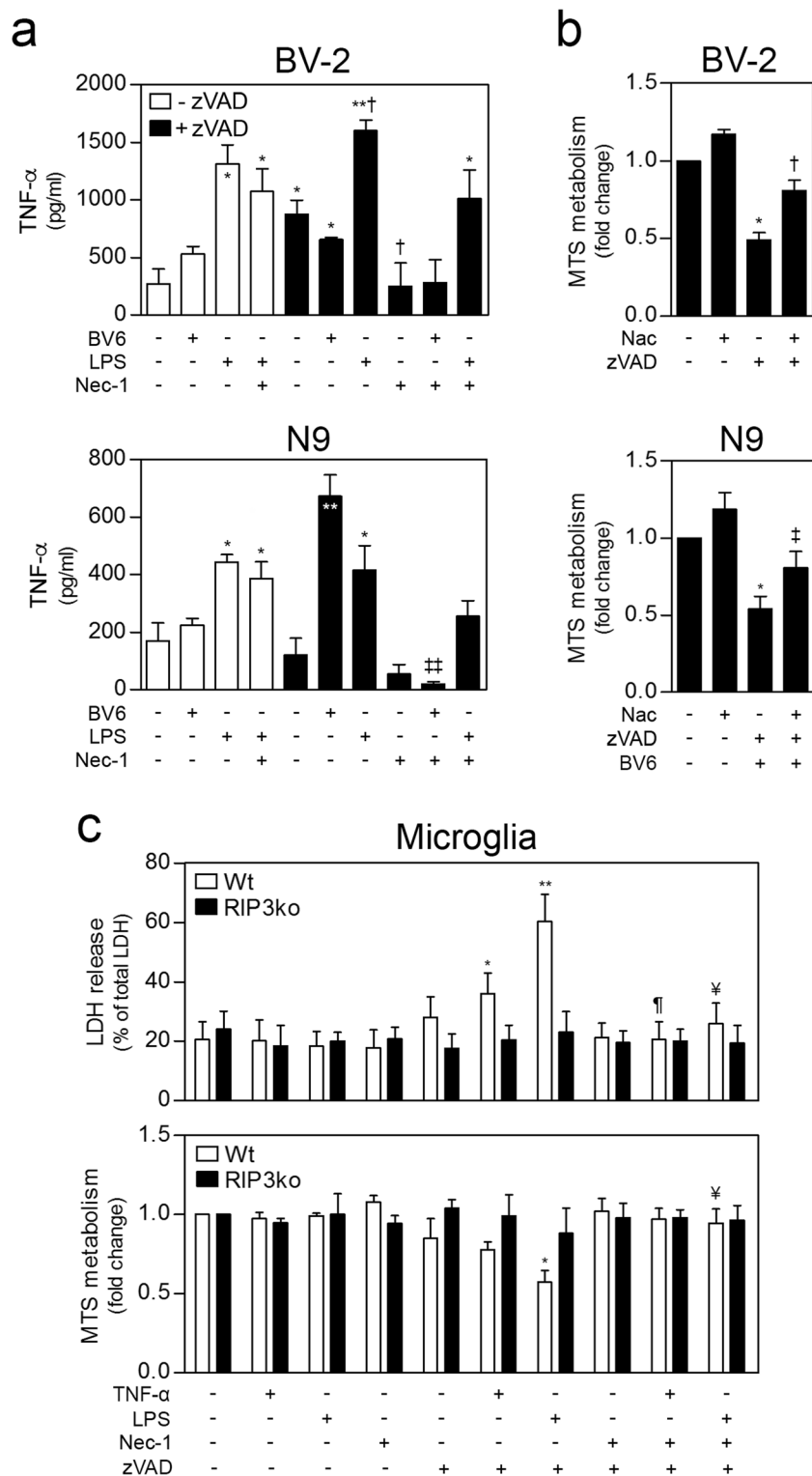


**Fig. 2** Evaluation of TNF- $\alpha$  secretion, cell death and viability in microglial cell lines and in primary microglia cells. **a** BV-2 and N9 microglia cells were exposed for 5 h to combinations of the following stimuli: 25  $\mu$ M zVAD, 0.5  $\mu$ M BV6, 10 ng/mL TNF- $\alpha$ , 100 ng/mL LPS, and 30  $\mu$ M Nec-1. TNF- $\alpha$  secretion to the culture supernatant was determined with a sandwich ELISA procedure. **b** BV-2 and N9 cells were co-treated with combinations of 25  $\mu$ M zVAD, 0.5  $\mu$ M BV6 and 1 mM Nac for 24 h, and cell metabolism was evaluated using the MTS assay. **c** Primary microglia cells isolated from wild-type (Wt) and RIP3 knockout (RIP3ko) mice were treated for 24 h with combinations of the following stimuli:

25  $\mu$ M zVAD, 10 ng/mL TNF- $\alpha$ , 100 ng/mL LPS and 30  $\mu$ M Nec-1, and cell membrane permeabilization and cell metabolism were evaluated by LDH and MTS assays, respectively. Values represent mean  $\pm$  SEM of three independent experiments. \* $p$  < 0.05 and \*\* $p$  < 0.01 from control, † $p$  < 0.05 from zVAD, ‡ $p$  < 0.05 from zVAD + BV6, †† $p$  < 0.01 from zVAD + BV6, ¶ $p$  < 0.05 from TNF- $\alpha$  + zVAD, and ¥ $p$  < 0.05 from LPS + zVAD. **a**, **c** Data were analyzed by one-way ANOVA followed by Tukey's post hoc test. **b** Data were analyzed by one-way ANOVA followed by Bonferroni's post hoc test

secretion upon exposure of BV-2 cells to zVAD alone or in combination with BV6. Incubation with LPS or LPS + zVAD further induced TNF- $\alpha$  production. In N9 cells, on the other hand, only co-incubation of zVAD with BV6 was sufficient to increase TNF- $\alpha$  secretion. Of note, zVAD or zVAD + BV6 exposure for 5 h did not lead to significantly higher LDH release in BV-2 and N9 cells, respectively, indicating that cell death is not the main mechanism for zVAD-dependent TNF- $\alpha$  secretion (data not shown). Finally, Nec-1 co-treatment completely reverted TNF- $\alpha$  secretion in both cell lines.

To evaluate the role of ROS, we co-incubated BV-2 and N9 cells treated with zVAD or zVAD + BV6, respectively, with Nac, a potent anti-oxidant molecule [35], for 24 h (Fig. 2b). Nac protected in ~30% from zVAD or zVAD + BV6 loss of cell viability. Moreover, Nac partially reverted loss of cell number and morphology detected with either zVAD or zVAD + BV6 (Supplementary Fig. 2). In contrast, Nac co-treatment did not alter membrane permeability, suggesting a latter role for ROS production (data not shown).

Finally, we evaluated necroptosis induction in primary microglia cultures prepared from Wt and RIP3ko mice, whose cells are devoid of necroptosis (Fig. 2c) [36]. Here, caspase inhibition with zVAD was insufficient to trigger necroptosis in primary Wt microglia, which in turn only occurred after co-incubation of zVAD with LPS or TNF- $\alpha$ . Finally, co-incubation with Nec-1 or RIP3ko totally protected from cell death.

### zVAD-Dependent Necroptosis Relies on RIP1/RIP3 Necrosome Assembly and MLKL Phosphorylation

To further confirm the involvement of necroptotic signaling pathways in zVAD-induced cell death, RIP1/RIP3 necrosome assembly and MLKL phosphorylation were evaluated as markers of necroptosis (Fig. 3). Treatment of BV-2 cells with zVAD induced RIP1/RIP3 necrosome assembly, as observed by RIP1 and RIP3 sequestration from the soluble to the insoluble fraction, along with a striking increase in phosphorylated MLKL (p-MLKL) in both fractions (Fig. 3a). For N9 cells, zVAD + BV6 also induced sequestration of RIP1 and RIP3 in the insoluble fraction and a marked increase in p-MLKL levels, followed by LPS + zVAD. Once again, co-treatment with Nec-1 totally abrogated these events. We also analyzed p-MLKL in total protein extracts from BV-2 and N9 cells stimulated for 5 h with a set of zVAD combinations. In fact, zVAD + BV6 already majorly increased p-MLKL levels in BV-2 cells, followed by zVAD alone (Fig. 3b). For N9 cells, zVAD + BV6 was also the strongest inducer of MLKL phosphorylation, followed by LPS + zVAD. Nec-1 co-incubation fully reverted these results. Overall, we confirmed RIP1/RIP3 necrosome formation and MLKL phosphorylation during necroptosis in BV-2 and N9 cells.

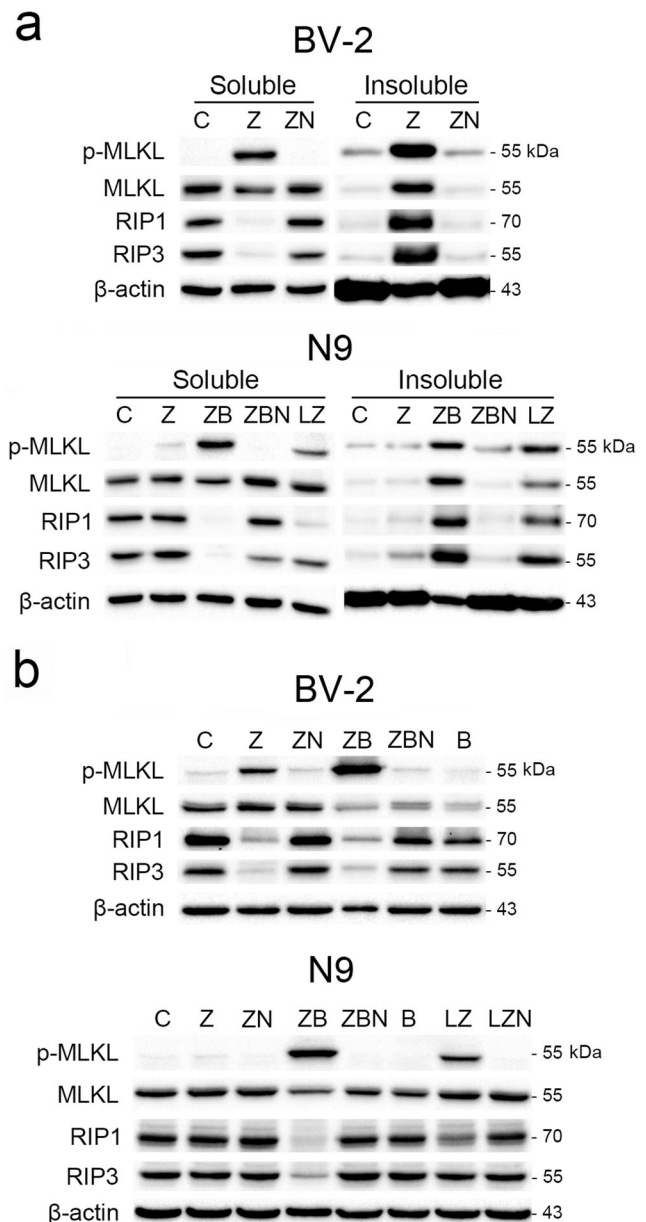
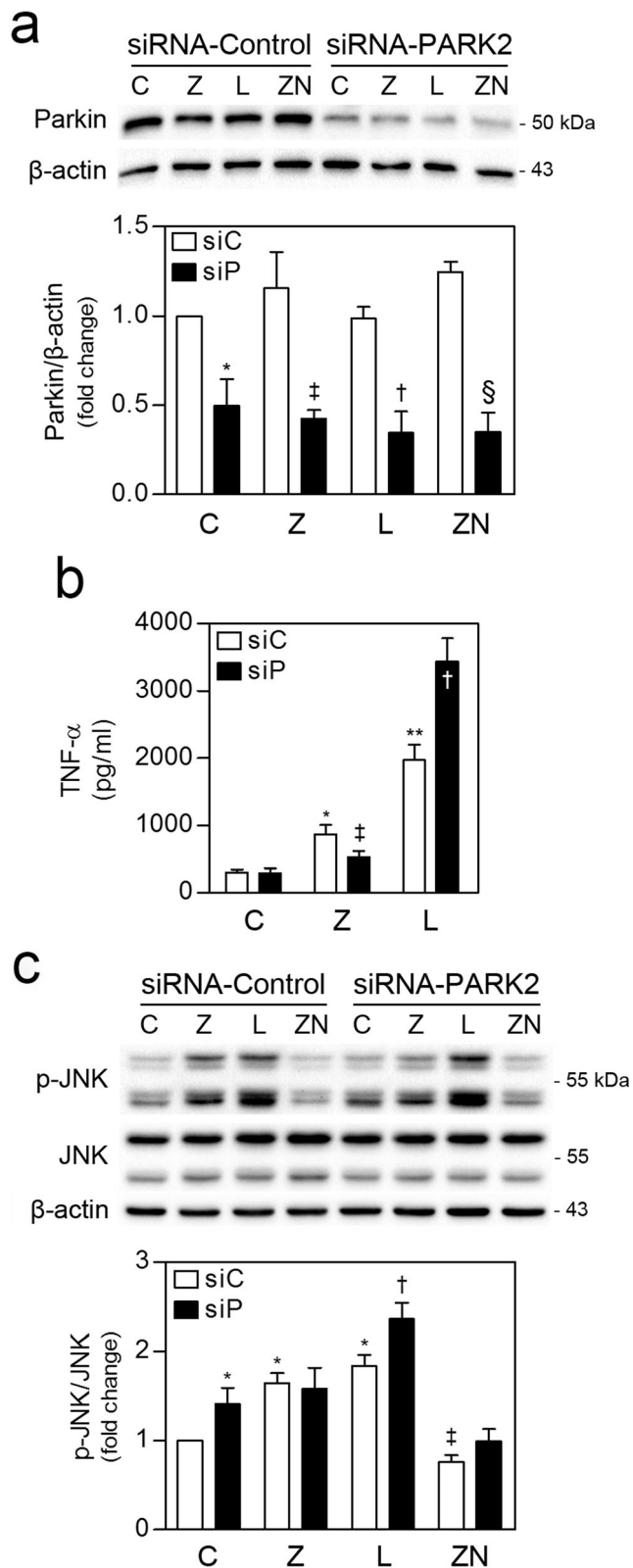


**Fig. 3** zVAD-induced necroptosis depends on RIP1/RIP3 necrosome assembly and MLKL phosphorylation in BV-2 and N9 microglia cells. **a** Cells were exposed to combinations of 25  $\mu$ M zVAD (Z), 0.5  $\mu$ M BV6 (B), and 30  $\mu$ M Nec-1 (N) for 8 h and RIP1/RIP3/MLKL sequestration in insoluble protein fractions was evaluated. **b** MLKL phosphorylation was further compared in total BV-2 and N9 cell lysates exposed to combinations of 25  $\mu$ M zVAD (Z), 0.5  $\mu$ M BV6 (B), 100 ng/mL LPS (L), and 30  $\mu$ M Nec-1 (N) for 5 h. Blots are representative of three independent experiments. C, control no addition

### Parkin Plays Different Roles during Necroptosis and Inflammation

Parkin can interact synergistically with LUBAC, a complex known to increase RIP1 linear ubiquitination [6, 37]. In turn, RIP1 linear ubiquitination is thought to stabilize complex I in detriment of cell death-inducing complexes [13, 17, 37, 38]. Therefore, we hypothesized that parkin decreases necroptosis



in microglial cells while influencing inflammation. We started by performing siRNA-mediated knockdown of parkin in BV-2 cells for 48 h, followed by 8 h of exposure to zVAD, LPS, or no addition (Fig. 4a). Parkin levels decreased in ~50% when

◀ **Fig. 4** Parkin silencing increases JNK phosphorylation and TNF- $\alpha$  secretion in LPS-treated cells. **a** Parkin siRNA-mediated knockdown was determined by Western blot in siRNA-Control (siC) and siRNA-PARK2 (siP) transfected BV-2 cells after exposure to combinations of 25  $\mu$ M zVAD (Z), 100 ng/mL LPS (L), and 30  $\mu$ M Nec-1 (N) for 8 h. **b** siC and siP transfected BV-2 cells were exposed to 25  $\mu$ M zVAD or 100 ng/mL LPS for 5 h, and TNF- $\alpha$  secretion to the culture supernatant was determined with a sandwich ELISA procedure. **c** JNK phosphorylation levels were determined in protein lysates from siC or siP transfected BV-2 cells exposed to combinations of 25  $\mu$ M zVAD (Z), 100 ng/mL LPS (L), and 30  $\mu$ M Nec-1 (N) for 8 h. Values represent mean  $\pm$  SEM of three independent experiments. \* $p$  < 0.05 and \*\* $p$  < 0.01 from siC, <sup>†</sup> $p$  < 0.05 from siC + LPS, <sup>‡</sup> $p$  < 0.05 from siC + zVAD and <sup>§</sup> $p$  < 0.05 from siC + ZN in one-way ANOVA followed by Tukey's post hoc test. C, control no addition

compared to cells transfected with a non-specific pool of siRNAs (siRNA-control). Moreover, parkin knockdown in BV-2 cells treated with zVAD significantly decreased TNF- $\alpha$  secretion, while the opposite was obtained after LPS exposure (Fig. 4b), suggesting that parkin exhibit opposite roles during these two cellular processes. Since LPS- and zVAD-driven TNF- $\alpha$  secretion may depend on the activation of MAPKs [33, 39, 40], we evaluated whether parkin silencing modulates JNK, p38, and Erk1/2 signaling pathways. As expected, exposure of BV-2 cells to LPS showed increased phosphorylation of all kinases (data not shown). zVAD significantly elevated JNK phosphorylation (Fig. 4c). Notably, compared to siRNA-Control transfected cells, parkin silencing further increased JNK phosphorylation levels in the presence or absence of LPS.

To further investigate whether the effects in TNF- $\alpha$  secretion were dependent on altered inflammatory responses after LPS or zVAD exposure, we evaluated mRNA levels of several pro-inflammatory mediators 8 h after exposure to LPS or zVAD. Overall, we observed a significant decrease of TNF- $\alpha$ , interleukin (IL)-1 $\beta$ , IL-6, and inducible nitric oxide synthase (iNOS) mRNA in siRNA-PARK2 transfected cells following zVAD exposure (Fig. 5a), while an opposite result was obtained for LPS-treated cells (Fig. 5b), again suggesting alternative roles for parkin in zVAD- and LPS-mediated inflammation. Of note, Nec-1 co-incubation totally abrogated pro-inflammatory gene expression (Supplementary Fig. 3), which has been recently demonstrated to be dependent on the recruitment of the necroptotic machinery [41].

### Parkin Silencing Attenuates Necroptosis Progression

Unexpectedly, parkin knockdown decreased LDH release by 40%, while totally abrogating zVAD-mediated reduction in MTS metabolism at 24 h post-zVAD treatment (Fig. 6a), which was also observed for 8 h (Fig. 6b). Moreover, MLKL phosphorylation was strongly reduced in siRNA-PARK2 transfected cells treated with zVAD, further confirming decreased necroptotic commitment (Fig. 6c). Co-

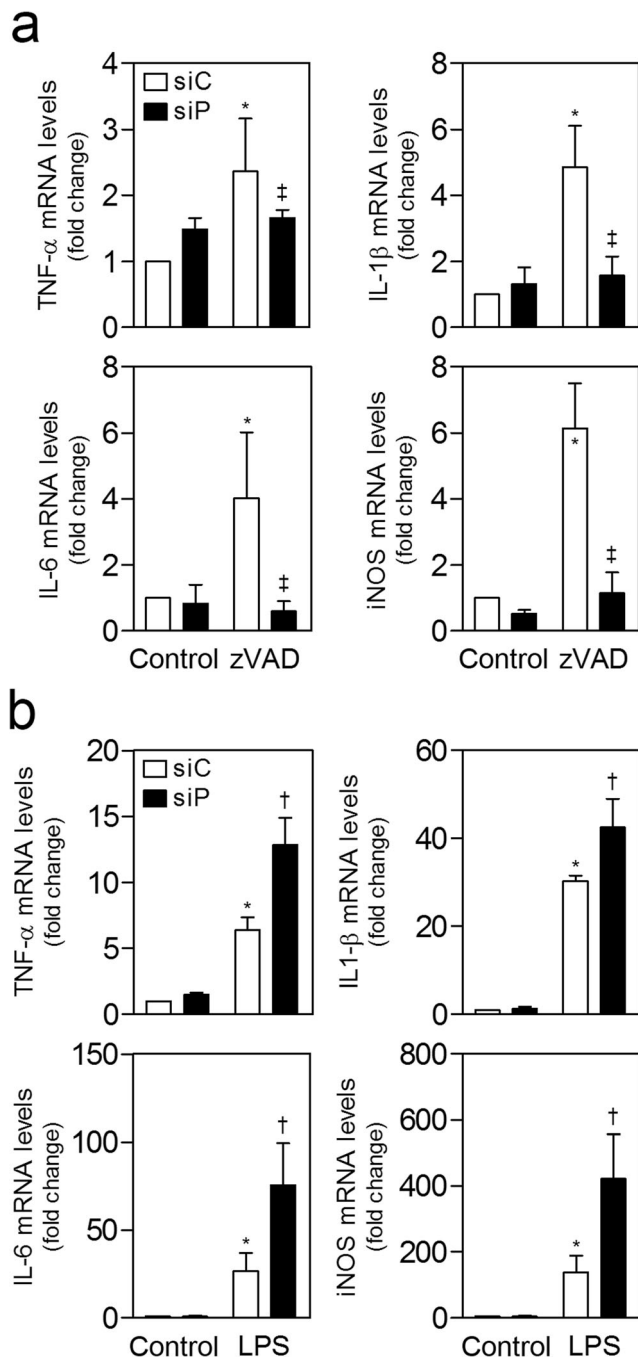


**Fig. 5** Parkin silencing differentially modulates pro-inflammatory gene expression following LPS or zVAD treatment. siRNA-Control (siC) or siRNA-PARK2 (siP) transfected BV-2 cells were exposed for 8 h to 25  $\mu$ M zVAD (a) or 100 ng/mL LPS (b), and TNF- $\alpha$ , IL-1 $\beta$ , IL-6 and iNOS mRNA levels were determined by qRT-PCR. Values represent mean  $\pm$  SEM of 4 independent experiments. \* $p$  < 0.05 from siC,  $\ddagger p$  < 0.05 from siC + LPS, and  $\ddagger p$  < 0.05 from siC + zVAD in one-way ANOVA followed by Bonferroni's post hoc test

incubation of zVAD with LPS abrogated siRNA-PARK2-mediated protection from necroptosis (data not shown), which is not surprising, considering that parkin knockdown may not affect TLR4-dependent necroptosis. Curiously, LPS exposure increased MLKL protein levels (Supplementary Fig. 4),

suggesting that LPS-stimulated cells are more prone to undergo necroptosis [16, 42].

Taking into account the role of parkin as an important component for mitophagy induction, we evaluated mitochondrial ROS production in siRNA-PARK2 and siRNA-Control transfected BV-2 cells treated with zVAD followed by incubation with the MitoSOX<sup>TM</sup> Red reagent. Surprisingly, no significant alterations were detected in any conditions tested (Supplementary Fig. 5a), suggesting that mitochondrial dynamics and ROS production are not involved in the protective effect of parkin knockdown. To further explore the molecular pathways involved in parkin-dependent necroptosis, we evaluated TRAF2/6 protein levels, since they are well-known targets of parkin involved in RIP1 polyubiquitination [12, 14, 17]. However, parkin silencing did not alter TRAF2/6 protein levels, either alone or in combination with zVAD or LPS (data not shown). We then explored a potential role for NF- $\kappa$ B, since higher activity of NF- $\kappa$ B protects from zVAD-dependent necroptosis [33]. However, NF- $\kappa$ B transcriptional activity remained unaltered between siRNA-Control and siRNA-PARK2 transfected cells (data not shown).

Finally, since higher RIP1 polyubiquitination may attenuate RIP1-dependent necroptosis [13, 14, 17, 43], we assessed RIP1 ubiquitination by performing immunoprecipitation of RIP1 from lysates of parkin-silenced cells treated with zVAD, followed by ubiquitin detection. Parkin silencing markedly increased RIP1-linked ubiquitin moieties levels after zVAD exposure (Fig. 6d), thus implicating RIP1 polyubiquitination status as a probable explanation for the mitigation of zVAD-induced necroptosis. Next, we evaluated the role of parkin during necroptosis in N9 and primary microglia. However, parkin knockdown in N9 cells did not affect LPS + zVAD- or zVAD + BV6-mediated necroptosis (data not shown). Of note, BV6 leads to reduced polyubiquitination of RIP1 and subsequent destabilization of complex I [17]. Regarding primary microglia, parkin knockdown was less efficient, with only  $\sim$ 40% reduction in parkin protein levels after siRNA-PARK2 transfection (Supplementary Fig. 6). Further, parkin silencing did not significantly protect from TNF- $\alpha$  + zVAD- or LPS + zVAD-induced necroptosis (Supplementary Fig. 6). These results unravel novel roles for parkin during necroptosis that are probably dependent on altered ubiquitination events.

### Parkin Knockdown Increases LPS-Driven pro-Inflammatory Response

Exposure to LPS has been shown to decrease parkin expression in BV-2 and primary microglia [11]. Therefore, we evaluated parkin protein levels in BV-2 and N9 microglial cells after exposure to LPS for 48 and 72 h (Fig. 7a). Importantly, the presence of LPS induced a marked decrease of parkin in all conditions tested. To further dissect the role of JNK in siRNA-PARK2 transfected cells in inflammation, we performed a

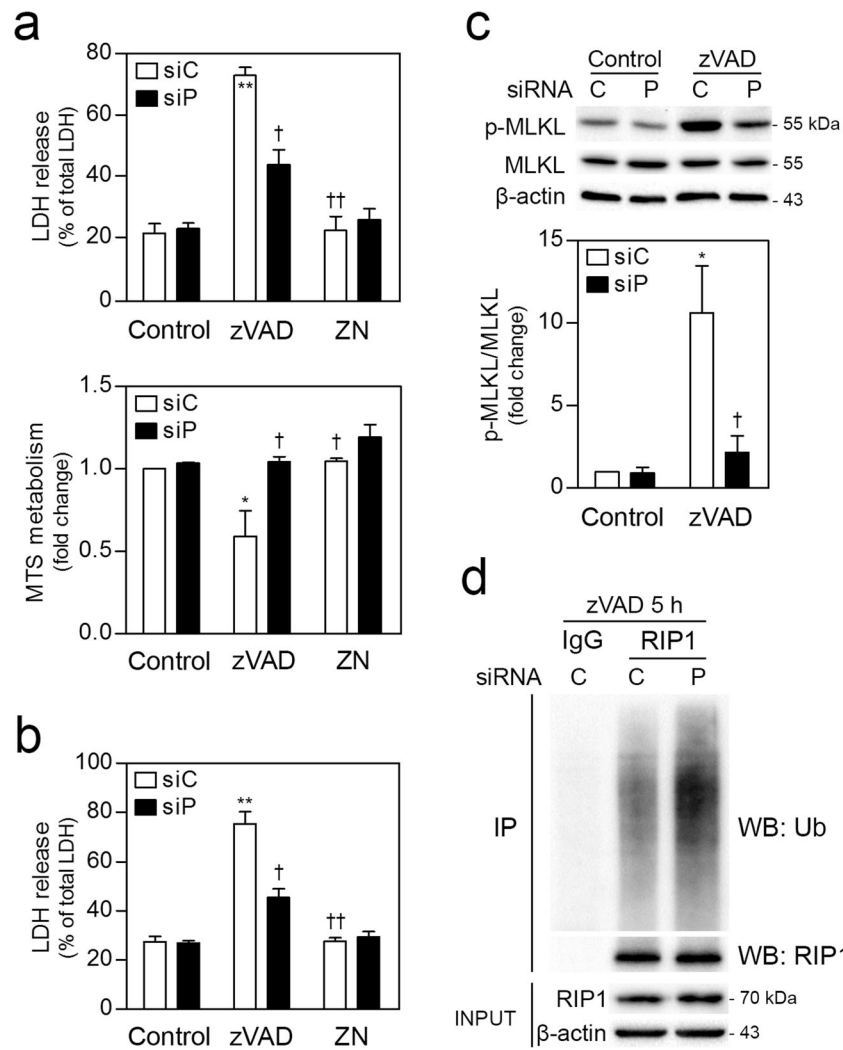


**Fig. 6** Parkin silencing attenuates necroptosis progression. siRNA-Control (siC) and siRNA-PARK2 (siP) transfected BV-2 cells were exposed to combinations of 25  $\mu$ M zVAD (Z) and 30  $\mu$ M Nec-1 (N) for 24 h (**a**) or 8 h (**b**) and cell membrane permeabilization and cell metabolism were evaluated by LDH and MTS assays, respectively. Values represent mean  $\pm$  SEM of four independent experiments. **c** siC and siP transfected BV-2 cells were exposed to 25  $\mu$ M zVAD (Z) and 30  $\mu$ M Nec-1 (N) for 8 h and MLKL phosphorylation levels were evaluated by Western blot.

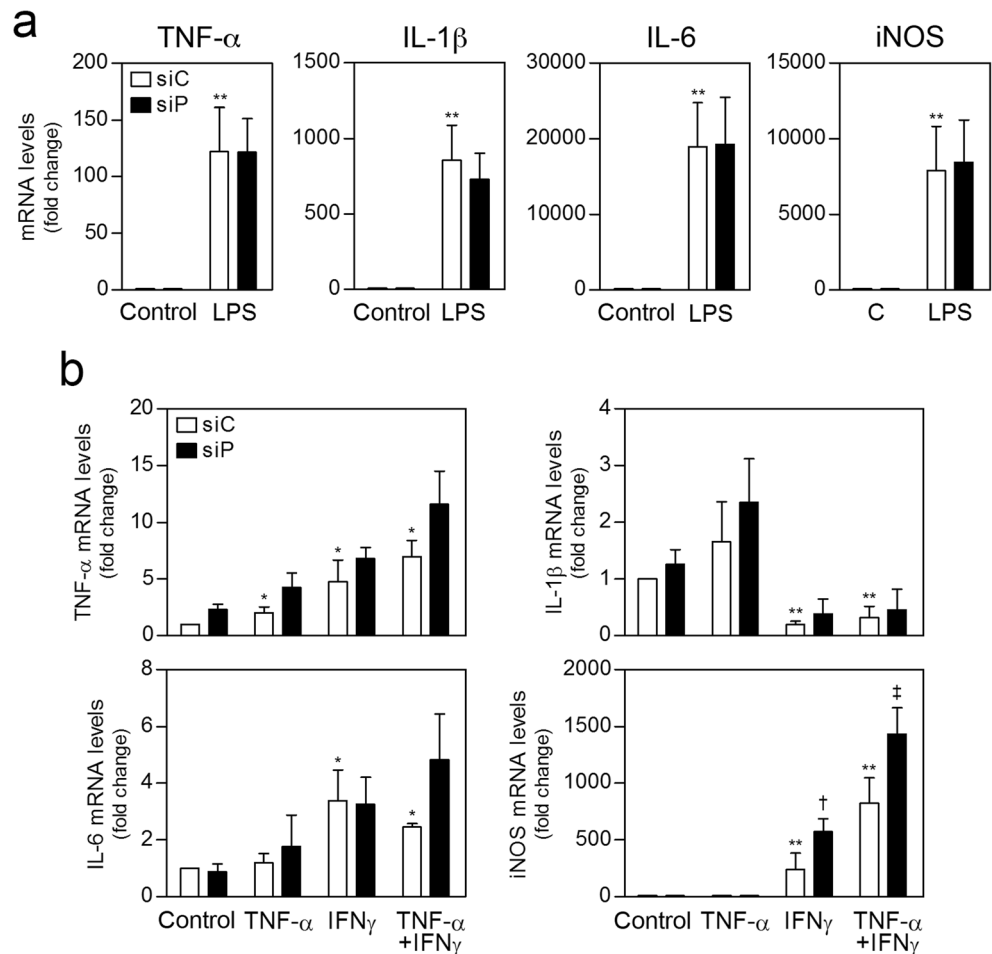
Values represent mean  $\pm$  SEM of three independent experiments. **d** RIP1 polyubiquitination by Western blot was determined following RIP1 immunoprecipitation from cell lysates of siC and siP transfected BV-2 cells exposed to 25  $\mu$ M zVAD for 5 h. Blots are representative of three independent experiments with similar results. \* $p < 0.05$  and \*\* $p < 0.01$  from siC, † $p < 0.05$ , and †† $p < 0.01$  from siC + zVAD. **a, b** Data were analyzed by one-way ANOVA followed by Tukey's post hoc test. **c** Data were analyzed by one-way ANOVA followed by Bonferroni's post hoc test

time-course of JNK activation following LPS incubation (Fig. 7b). JNK was over-activated in cells with silenced parkin as early as 30 min after LPS incubation, which was maintained for 8 h. In turn, p38 and Erk1/2 phosphorylation levels were increased following LPS exposure but were not further augmented in siRNA-PARK2 transfected cells (data not shown). I $\kappa$ B phosphorylation also presented a tendency to increase in siRNA-PARK2 transfected cells stimulated with LPS when compared to siRNA-Control cells (Fig. 7c). Moreover, parkin silencing led to increased NF- $\kappa$ B transcriptional activity following LPS incubation (Fig. 7d). Therefore, increased expression of pro-inflammatory mediators may depend on NF- $\kappa$ B and activating protein 1 (AP-1), composed by c-Fos and phosphorylated c-Jun, the main JNK target.

Loss of parkin may also contribute to higher mitochondrial ROS levels, which can increase LPS-mediated inflammatory response in microglia [44–46]. Therefore, we assessed mitochondrial ROS in BV-2 cells with parkin knockdown treated with LPS or no addition (Supplementary Fig. 5b). Nevertheless, no changes were detected in cells with silenced parkin, suggesting that mitochondrial ROS are not involved in the higher pro-inflammatory response. Since RIP1 ubiquitination can contribute to mediate TLR4-dependent downstream signaling [47], we checked whether parkin silencing could have an effect on RIP1 polyubiquitination, but unexpectedly no differences were detected after LPS exposure both at 30 min and 5 h (data not shown).



**Fig. 8** Parkin silencing increases TNF- $\alpha$ /IFN $\gamma$  pro-inflammatory response in primary microglia. siRNA-Control (siC) and siRNA-PARK2 (siP) transfected primary microglia were exposed for 8 h to 100 ng/mL LPS (a) or combinations of 10 ng/mL TNF- $\alpha$ , 100 U/mL IFN $\gamma$  or TNF- $\alpha$  + IFN $\gamma$  (b), and TNF- $\alpha$ , IL-1 $\beta$ , IL-6, and iNOS mRNA levels were determined by qRT-PCR. Values represent mean  $\pm$  SEM of four independent experiments. \* $p$  < 0.05 and \*\* $p$  < 0.01 from siC, † $p$  < 0.05 from siC + IFN $\gamma$  and ‡ $p$  < 0.05 from siC + TNF- $\alpha$  + IFN $\gamma$ . a Data were analyzed by one-way ANOVA followed by Bonferroni's post hoc test. b Data were analyzed by one-way ANOVA followed by Tukey's post hoc test



display (EDD) physical interaction, which contributes to JNK and Erk 1/2 activation and subsequent AP1-dependent TNF- $\alpha$  expression [33, 34]. This mechanism is dependent on RIP1 kinase activity, since Nec-1 abolished TNF- $\alpha$  production [34]. We recapitulated these observations, since Nec-1 abolished TNF- $\alpha$  secretion in conditions leading to necroptosis, while zVAD exposure was also correlated with higher JNK and Erk1/2 activation in BV-2 cells. Interestingly, a Smac mimetic also contributes to TNF- $\alpha$  production by inducing RIP1 kinase activity in an EDD-dependent manner, which may explain why N9 cells require zVAD and BV6 to secrete more TNF- $\alpha$  [34]. Nevertheless, addition of exogenous TNF- $\alpha$  at 20 ng/mL in combination with zVAD only slightly induced necroptosis in N9 cells. Moreover, zVAD alone was a much stronger inducer of necroptosis in BV-2 cells than IETD, as previously observed for L929 cells, suggesting other mechanisms for zVAD-mediated sensitization to necroptosis [33].

We had also hypothesized that parkin plays a role in protecting from necroptosis. Surprisingly, we found that parkin knockdown in BV-2 cells markedly protected from all necroptotic-related effects. Although parkin is a regulator of mitophagy, and parkin knockdown could increase mitochondrial ROS, that was not the case in our model, thus

excluding a role for mitophagy in zVAD-mediated necroptosis. Moreover, anti-oxidant Nac could only partially revert late-stage loss of MTS metabolism without affecting membrane permeability, while parkin silencing reduced these two necroptotic aspects. Interestingly, despite the controversial roles of ROS production and mitochondria/mitophagy in necroptosis [31, 50–54], mitophagy can contribute to TNF- $\alpha$ -independent necroptosis by increasing mitochondrial ROS production [50, 51]. Conversely, parkin silencing does not affect TNF- $\alpha$ -dependent necroptosis in L929 cells [55], while parkin-induced mitochondrial depletion does not protect from necroptosis mediated by TNF- $\alpha$  + zVAD [31]. Overall, the importance of ROS and mitochondria during necroptosis appears to be cell type- and stimulus-dependent.

Importantly, parkin knockdown increased RIP1 polyubiquitination levels without affecting RIP1 total protein levels, therefore suggesting altered non-degradative ubiquitination signaling [4, 47]. In turn, higher RIP1 polyubiquitination levels are expected to stabilize RIP1 in pro-survival complex I, which may explain the reduction of zVAD-mediated necroptosis [14, 17]. However, the stabilizing roles of RIP1 linear and Lys63-linked ubiquitin chains have been recently challenged, despite cIAP2 being crucial to

complex I stabilization [14, 17, 38]. Here, we speculate that parkin may be influencing protein levels of one or more mediators that stabilize RIP1 ubiquitination, with the exclusion of TRAF2/6 that remained unaltered.

Of note, although JNK phosphorylation levels were not altered between zVAD-treated siRNA-Control and siRNA-PARK2 transfected cells, parkin silencing alone increased JNK phosphorylation not cumulative with zVAD-dependent JNK activation, which may indicate that parkin silencing decreases zVAD-mediated JNK activation. Regarding the role of necroptosis in microglia, it has been reported that death of microglia by necroptosis contribute to multiple sclerosis progression [56]. However, necroptosis may reduce inflammation by limiting immune cell populations [15, 30, 42, 57]. Moreover, microglial necroptosis protects primary neurons against inflammation [30]. Therefore, it is possible that, by protecting microglia from cell death, parkin loss may allow for the maintenance of activated microglia that would otherwise perish.

Several reports implicate parkin as a regulator of inflammation, despite some controversy regarding its pro- or anti-inflammatory role [9–12]. Here, LPS exposure led to decreased parkin protein levels in BV-2 and N9 cells, an observation also described for BV-2 and primary microglia [11]. This effect may be dependent on *PARK2* transcriptional repression mediated by NF- $\kappa$ B [11]. We also observed NF- $\kappa$ B, as well as JNK, over-activation in BV-2 cells with silenced parkin following LPS exposure, which were correlated with higher pro-inflammatory gene expression and TNF- $\alpha$  secretion. Since phosphorylation of other MAPKs activated by LPS, such as p38 and Erk1/2, are not altered by *PARK2* knockdown, these effects are probably independent of direct altered TLR4 downstream signaling. Importantly, two other studies reported higher JNK phosphorylation levels following parkin knockdown in inflammatory settings, with one also showing higher NF- $\kappa$ B activity [9, 12]. Moreover, several other studies demonstrated increased JNK activity upon parkin downregulation or inactivation in non-inflammatory contexts [58–61]. Increased JNK activity has been linked to ROS production, which in turn is elevated upon accumulation of damaged mitochondria [5, 62]. However, we did not observe any differences in mitochondrial ROS levels between siRNA-control and siRNA-PARK2 transfected cells unstimulated or stimulated with LPS. Moreover, RIP1 polyubiquitination levels were unaltered in BV-2 cells treated with LPS, suggesting that the higher pro-inflammatory response detected in this cell model after parkin knockdown is independent on altered RIP1-downstream signaling. Finally, primary microglia with decreased parkin levels presented higher expression of pro-inflammatory genes in mild pro-inflammatory conditions, closer to PD-derived neuroinflammation. Overall, our results support an anti-inflammatory role for parkin, probably by limiting NF- $\kappa$ B and JNK responses.

In conclusion, we unravel unsuspected roles for parkin during necroptosis and inflammation in microglia, which are probably dependent on altered ubiquitination events. Here, parkin silencing protected from zVAD-mediated necroptosis, while potentiating LPS-induced inflammation by elevating NF- $\kappa$ B and JNK activities. These observations suggest that loss of parkin may contribute to higher microglial survival and pro-inflammatory activation in PD, which could contribute to PD pathogenesis through chronic neuroinflammation.

**Acknowledgements** This work was supported by Fundação para a Ciência e a Tecnologia (FCT) through iMed.ULisboa grant UID/DTP/04138/2013 and individual fellowships SFRH/BPD/100961/2014, PD/BD/128332/2017 and SFRH/BD/102771/2014.

## Compliance with Ethical Standards

**Conflict of Interest** The authors declare that they have no conflict of interest.

## References

- Poewe W, Seppi K, Tanner CM, Halliday GM, Brundin P, Volkman J, Schrag AE, Lang AE (2017) Parkinson disease. *Nat Rev Dis Primers* 3:17013. <https://doi.org/10.1038/nrdp.2017.13>
- Henn IH, Gostner JM, Lackner P, Tatzelt J, Winklhofer KF (2005) Pathogenic mutations inactivate parkin by distinct mechanisms. *J Neurochem* 92(1):114–122. <https://doi.org/10.1111/j.1471-4159.2004.02854.x>
- Klein C, Lohmann-Hedrich K, Rogaeva E, Schlossmacher MG, Lang AE (2007) Deciphering the role of heterozygous mutations in genes associated with parkinsonism. *Lancet Neurol* 6(7):652–662. [https://doi.org/10.1016/S1474-4422\(07\)70174-6](https://doi.org/10.1016/S1474-4422(07)70174-6)
- Dawson TM, Dawson VL (2010) The role of parkin in familial and sporadic Parkinson's disease. *Mov Disord* 25(Suppl 1):S32–S39. <https://doi.org/10.1002/mds.22798>
- Seirafi M, Kozlov G, Gehring K (2015) Parkin structure and function. *FEBS J* 282(11):2076–2088. <https://doi.org/10.1111/febs.13249>
- Muller-Rischart AK, Pils A, Beaudette P et al (2013) The E3 ligase parkin maintains mitochondrial integrity by increasing linear ubiquitination of NEMO. *Mol Cell* 49(5):908–921. <https://doi.org/10.1016/j.molcel.2013.01.036>
- Henn IH, Bouman L, Schlehe JS, Schlierf A, Schramm JE, Wegener E, Nakaso K, Culmsee C et al (2007) Parkin mediates neuroprotection through activation of IkappaB kinase/nuclear factor-kappaB signaling. *J Neurosci* 27(8):1868–1878. <https://doi.org/10.1523/JNEUROSCI.5537-06.2007>
- Manzanillo PS, Ayres JS, Watson RO, Collins AC, Souza G, Rae CS, Schneider DS et al (2013) The ubiquitin ligase parkin mediates resistance to intracellular pathogens. *Nature* 501(7468):512–516. <https://doi.org/10.1038/nature12566>
- de Leseleuc L, Orlova M, Cobat A et al (2013) PARK2 mediates interleukin 6 and monocyte chemoattractant protein 1 production by human macrophages. *PLoS Negl Trop Dis* 7(1):e2015. <https://doi.org/10.1371/journal.pntd.0002015>
- Letsiou E, Sammani S, Wang H, Belvitch P, Dudek SM (2017) Parkin regulates lipopolysaccharide-induced proinflammatory responses in acute lung injury. *Transl Res* 181:71–82. <https://doi.org/10.1016/j.trsl.2016.09.002>

11. Tran TA, Nguyen AD, Chang J, Goldberg MS, Lee JK, Tansey MG (2011) Lipopolysaccharide and tumor necrosis factor regulate Parkin expression via nuclear factor-kappa B. *PLoS One* 6(8): e23660. <https://doi.org/10.1371/journal.pone.0023660>
12. Chung JY, Park HR, Lee SJ, Lee SH, Kim JS, Jung YS, Hwang SH, Ha NC et al (2013) Elevated TRAF2/6 expression in Parkinson's disease is caused by the loss of Parkin E3 ligase activity. *Lab Invest* 93(6):663–676. <https://doi.org/10.1038/labinvest.2013.60>
13. Haas TL, Emmerich CH, Gerlach B, Schmukle AC, Cordier SM, Rieser E, Feltham R, Vince J et al (2009) Recruitment of the linear ubiquitin chain assembly complex stabilizes the TNF-R1 signaling complex and is required for TNF-mediated gene induction. *Mol Cell* 36(5):831–844. <https://doi.org/10.1016/j.molcel.2009.10.013>
14. Ofengeim D, Yuan J (2013) Regulation of RIP1 kinase signalling at the crossroads of inflammation and cell death. *Nat Rev Mol Cell Biol* 14(11):727–736. <https://doi.org/10.1038/nrm3683>
15. Kearney CJ, Martin SJ (2017) An inflammatory perspective on necroptosis. *Mol Cell* 65(6):965–973. <https://doi.org/10.1016/j.molcel.2017.02.024>
16. Kim SJ, Li J (2013) Caspase blockade induces RIP3-mediated programmed necrosis in toll-like receptor-activated microglia. *Cell Death Dis* 4:e716. <https://doi.org/10.1038/cddis.2013.238>
17. Liu X, Shi F, Li Y, Yu X, Peng S, Li W, Luo X, Cao Y (2016) Post-translational modifications as key regulators of TNF-induced necroptosis. *Cell Death Dis* 7(7):e2293. <https://doi.org/10.1038/cddis.2016.197>
18. Li J, McQuade T, Siemer AB, Napetschnig J, Moriwaki K, Hsiao YS, Damko E, Moquin D et al (2012) The RIP1/RIP3 necrosome forms a functional amyloid signaling complex required for programmed necrosis. *Cell* 150(2):339–350. <https://doi.org/10.1016/j.cell.2012.06.019>
19. Wang H, Sun L, Su L, Rizo J, Liu L, Wang LF, Wang FS et al (2014) Mixed lineage kinase domain-like protein MLKL causes necrotic membrane disruption upon phosphorylation by RIP3. *Mol Cell* 54(1):133–146. <https://doi.org/10.1016/j.molcel.2014.03.003>
20. Caccamo A, Branca C, Piras IS, Ferreira E, Huentelman MJ, Liang WS, Readhead B, Dudley JT et al (2017) Necroptosis activation in Alzheimer's disease. *Nat Neurosci* 20(9):1236–1246. <https://doi.org/10.1038/nn.4608>
21. Iannielli A, Bido S, Folladori L, Segnali A, Cancellieri C, Maresca A, Massimino L, Rubio A et al (2018) Pharmacological inhibition of necroptosis protects from dopaminergic neuronal cell death in Parkinson's disease models. *Cell Rep* 22(8):2066–2079. <https://doi.org/10.1016/j.celrep.2018.01.089>
22. Blasi E, Barluzzi R, Bocchini V, Mazzolla R, Bistoni F (1990) Immortalization of murine microglial cells by a v-raf/v-myc carrying retrovirus. *J Neuroimmunol* 27(2–3):229–237
23. Righi M, Mori L, De Libero G et al (1989) Monokine production by microglial cell clones. *Eur J Immunol* 19(8):1443–1448. <https://doi.org/10.1002/eji.1830190815>
24. Nikodemova M, Watters JJ (2011) Outbred ICR/CD1 mice display more severe neuroinflammation mediated by microglial TLR4/CD14 activation than inbred C57Bl/6 mice. *Neuroscience* 190: 67–74. <https://doi.org/10.1016/j.neuroscience.2011.06.006>
25. Gordo AC, Falcao AS, Fernandes A, Brito MA, Silva RF, Brites D (2006) Unconjugated bilirubin activates and damages microglia. *J Neurosci Res* 84(1):194–201. <https://doi.org/10.1002/jnr.20857>
26. Saura J, Tusell JM, Serratosa J (2003) High-yield isolation of murine microglia by mild trypsinization. *Glia* 44(3):183–189. <https://doi.org/10.1002/glia.10274>
27. Witting A, Moller T (2011) Microglia cell culture: a primer for the novice. *Methods Mol Biol* 758:49–66. [https://doi.org/10.1007/978-1-61779-170-3\\_4](https://doi.org/10.1007/978-1-61779-170-3_4)
28. Pereira DM, Simoes AE, Gomes SE et al (2016) MEK5/ERK5 signaling inhibition increases colon cancer cell sensitivity to 5-fluorouracil through a p53-dependent mechanism. *Oncotarget* 7(23):34322–34340. <https://doi.org/10.18632/oncotarget.9107>
29. Wu CH, Fallini C, Ticozzi N, Keagle PJ, Sapp PC, Piotrowska K, Lowe P, Koppers M et al (2012) Mutations in the profilin 1 gene cause familial amyotrophic lateral sclerosis. *Nature* 488(7412): 499–503. <https://doi.org/10.1038/nature11280>
30. Fricker M, Vilalta A, Tolkovsky AM, Brown GC (2013) Caspase inhibitors protect neurons by enabling selective necroptosis of inflamed microglia. *J Biol Chem* 288(13):9145–9152. <https://doi.org/10.1074/jbc.M112.427880>
31. Tait SW, Oberst A, Quarato G et al (2013) Widespread mitochondrial depletion via mitophagy does not compromise necroptosis. *Cell Rep* 5(4):878–885. <https://doi.org/10.1016/j.celrep.2013.10.034>
32. Bernas T, Dobrucki J (2002) Mitochondrial and nonmitochondrial reduction of MTT: Interaction of MTT with TMRE, JC-1, and NAO mitochondrial fluorescent probes. *Cytometry* 47(4):236–242
33. Wu YT, Tan HL, Huang Q, Sun XJ, Zhu X, Shen HM (2011) zVAD-induced necroptosis in L929 cells depends on autocrine production of TNFalpha mediated by the PKC-MAPKs-AP-1 pathway. *Cell Death Differ* 18(1):26–37. <https://doi.org/10.1038/cdd.2010.72>
34. Christofferson DE, Li Y, Hitomi J, Zhou W, Upperman C, Zhu H, Gerber SA, Gygi S et al (2012) A novel role for RIP1 kinase in mediating TNFalpha production. *Cell Death Dis* 3:e320. <https://doi.org/10.1038/cddis.2012.64>
35. Kerksick C, Willoughby D (2005) The antioxidant role of glutathione and N-acetyl-cysteine supplements and exercise-induced oxidative stress. *J Int Soc Sports Nutr* 2:38–44. <https://doi.org/10.1186/1550-2783-2-2-38>
36. Afonso MB, Rodrigues PM, Carvalho T, Caridade M, Borralho P, Cortez-Pinto H, Castro RE, Rodrigues CMP (2015) Necroptosis is a key pathogenic event in human and experimental murine models of non-alcoholic steatohepatitis. *Clin Sci (Lond)* 129(8):721–739. <https://doi.org/10.1042/CS20140732>
37. Gerlach B, Cordier SM, Schmukle AC, Emmerich CH, Rieser E, Haas TL, Webb AI, Rickard JA et al (2011) Linear ubiquitination prevents inflammation and regulates immune signalling. *Nature* 471(7340):591–596. <https://doi.org/10.1038/nature09816>
38. de Almagro MC, Goncharov T, Newton K, Vucic D (2015) Cellular IAP proteins and LUBAC differentially regulate necrosome-associated RIP1 ubiquitination. *Cell Death Dis* 6:e1800. <https://doi.org/10.1038/cddis.2015.158>
39. Kawai T, Akira S (2010) The role of pattern-recognition receptors in innate immunity: Update on toll-like receptors. *Nat Immunol* 11(5):373–384. <https://doi.org/10.1038/ni.1863>
40. Wang MJ, Huang HY, Chen WF, Chang HF, Kuo JS (2010) Glycogen synthase kinase-3beta inactivation inhibits tumor necrosis factor-alpha production in microglia by modulating nuclear factor kappaB and MLK3/JNK signaling cascades. *J Neuroinflammation* 7:99. <https://doi.org/10.1186/1742-2094-7-99>
41. Zhu K, Liang W, Ma Z, Xu D, Cao S, Lu X, Liu N, Shan B et al (2018) Necroptosis promotes cell-autonomous activation of proinflammatory cytokine gene expression. *Cell Death Dis* 9(5):500. <https://doi.org/10.1038/s41419-018-0524-y>
42. Li Z, Scott MJ, Fan EK, Li Y, Liu J, Xiao G, Li S, Billiar TR et al (2016) Tissue damage negatively regulates LPS-induced macrophage necroptosis. *Cell Death Differ* 23(9):1428–1447. <https://doi.org/10.1038/cdd.2016.21>
43. McComb S, Cheung HH, Korneluk RG, Wang S, Krishnan L, Sad S (2012) cIAP1 and cIAP2 limit macrophage necroptosis by inhibiting Rip1 and Rip3 activation. *Cell Death Differ* 19(11): 1791–1801. <https://doi.org/10.1038/cdd.2012.59>
44. Voloboueva LA, Emery JF, Sun X, Giffard RG (2013) Inflammatory response of microglial BV-2 cells includes a glycolytic shift and is modulated by mitochondrial glucose-regulated

- protein 75/mortalin. *FEBS Lett* 587(6):756–762. <https://doi.org/10.1016/j.febslet.2013.01.067>
45. Park J, Choi H, Min JS, Park SJ, Kim JH, Park HJ, Kim B, Chae JI et al (2013) Mitochondrial dynamics modulate the expression of pro-inflammatory mediators in microglial cells. *J Neurochem* 127(2):221–232. <https://doi.org/10.1111/jnc.12361>
  46. Bordt EA, Polster BM (2014) NADPH oxidase- and mitochondria-derived reactive oxygen species in proinflammatory microglial activation: a bipartisan affair? *Free Radic Biol Med* 76:34–46. <https://doi.org/10.1016/j.freeradbiomed.2014.07.033>
  47. Cusson-Hermance N, Khurana S, Lee TH, Fitzgerald KA, Kellihher MA (2005) Rip1 mediates the Trif-dependent toll-like receptor 3- and 4-induced NF- $\kappa$ B activation but does not contribute to interferon regulatory factor 3 activation. *J Biol Chem* 280(44):36560–36566. <https://doi.org/10.1074/jbc.M506831200>
  48. De Boer ML, Hu J, Kalvakolanu DV, Hasday JD, Cross AS (2001) IFN-gamma inhibits lipopolysaccharide-induced interleukin-1 beta in primary murine macrophages via a Stat1-dependent pathway. *J Interf Cytokine Res* 21(7):485–494. <https://doi.org/10.1089/10799900152434358>
  49. Ucla C, Roux-Lombard P, Fey S, Dayer JM, Mach B (1990) Interferon gamma drastically modifies the regulation of interleukin 1 genes by endotoxin in U937 cells. *J Clin Invest* 85(1):185–191. <https://doi.org/10.1172/JCI114411>
  50. Mizumura K, Cloonan SM, Nakahira K, Bhashyam AR, Cervo M, Kitada T, Glass K, Owen CA et al (2014) Mitophagy-dependent necroptosis contributes to the pathogenesis of COPD. *J Clin Invest* 124(9):3987–4003. <https://doi.org/10.1172/JCI74985>
  51. Basit F, van Oppen LM, Schockel L et al (2017) Mitochondrial complex I inhibition triggers a mitophagy-dependent ROS increase leading to necroptosis and ferroptosis in melanoma cells. *Cell Death Dis* 8(3):e2716. <https://doi.org/10.1038/cddis.2017.133>
  52. Zhang Y, Su SS, Zhao S, Yang Z, Zhong CQ, Chen X, Cai Q, Yang ZH et al (2017) RIP1 autophosphorylation is promoted by mitochondrial ROS and is essential for RIP3 recruitment into necrosome. *Nat Commun* 8:14329. <https://doi.org/10.1038/ncomms14329>
  53. Schenk B, Fulda S (2015) Reactive oxygen species regulate Smac mimetic/TNF $\alpha$ -induced necroptotic signaling and cell death. *Oncogene* 34(47):5796–5806. <https://doi.org/10.1038/onc.2015.35>
  54. Yang Z, Wang Y, Zhang Y, He X, Zhong CQ, Ni H, Chen X, Liang Y et al (2018) RIP3 targets pyruvate dehydrogenase complex to increase aerobic respiration in TNF-induced necroptosis. *Nat Cell Biol* 20(2):186–197. <https://doi.org/10.1038/s41556-017-0022-y>
  55. Remijsen Q, Goossens V, Grootjans S, van den Haute C, Vanlangenakker N, Dondelinger Y, Roelandt R, Bruggeman I et al (2014) Depletion of RIPK3 or MLKL blocks TNF-driven necroptosis and switches towards a delayed RIPK1 kinase-dependent apoptosis. *Cell Death Dis* 5:e1004. <https://doi.org/10.1038/cddis.2013.531>
  56. Ofengeim D, Ito Y, Najafav A, Zhang Y, Shan B, DeWitt JP, Ye J, Zhang X et al (2015) Activation of necroptosis in multiple sclerosis. *Cell Rep* 10(11):1836–1849. <https://doi.org/10.1016/j.celrep.2015.02.051>
  57. Kearney CJ, Cullen SP, Tynan GA, Henry CM, Clancy D, Lavelle EC, Martin SJ (2015) Necroptosis suppresses inflammation via termination of TNF- or LPS-induced cytokine and chemokine production. *Cell Death Differ* 22(8):1313–1327. <https://doi.org/10.1038/cdd.2014.222>
  58. Cha GH, Kim S, Park J, Lee E, Kim M, Lee SB, Kim JM, Chung J et al (2005) Parkin negatively regulates JNK pathway in the dopaminergic neurons of drosophila. *Proc Natl Acad Sci U S A* 102(29):10345–10350. <https://doi.org/10.1073/pnas.0500346102>
  59. Ren Y, Jiang H, Yang F, Nakaso K, Feng J (2009) Parkin protects dopaminergic neurons against microtubule-depolymerizing toxins by attenuating microtubule-associated protein kinase activation. *J Biol Chem* 284(6):4009–4017. <https://doi.org/10.1074/jbc.M806245200>
  60. Liu M, Aneja R, Sun X, Xie S, Wang H, Wu X, Dong JT, Li M et al (2008) Parkin regulates Eg5 expression by Hsp70 ubiquitination-dependent inactivation of c-Jun NH2-terminal kinase. *J Biol Chem* 283(51):35783–35788. <https://doi.org/10.1074/jbc.M806860200>
  61. Jiang H, Ren Y, Zhao J, Feng J (2004) Parkin protects human dopaminergic neuroblastoma cells against dopamine-induced apoptosis. *Hum Mol Genet* 13(16):1745–1754. <https://doi.org/10.1093/hmg/ddh180>
  62. Shen HM, Liu ZG (2006) JNK signaling pathway is a key modulator in cell death mediated by reactive oxygen and nitrogen species. *Free Radic Biol Med* 40(6):928–939. <https://doi.org/10.1016/j.freeradbiomed.2005.10.056>